Electronic Supplementary Information

Controlling receptor function from the extracellular vestibule of G-protein coupled receptors

Attila Egyed,[a] Katalin Domány-Kovács,[b] Bence Koványi,[b] Ferenc Horti,[b] Dalma Kurkó,[b] Dóra Judit Kiss,[a] Gáspár Pándy-Szekeres,[a] István Greiner [b] and György M. Keserű *[a]

[a] *Medicinal Chemistry Research Group, Research Center for Natural Sciences Magyar tudósok krt. 2, Budapest, H-1117, Hungary Email: keseru.gyorgy@ttk.mta.hu*

[b] *Gedeon Richter plc Gyömrői út 19-21, Budapest, H-1103, Hungary*

DOI:

Table of Contents

1. Experimental Procedures

NMR spectra were recorded in CD_3OD or DMSO-d_6 solution at 30 °C, on a Varian Unity Inova 500 spectrometer (500 MHz for ^1H NMR and 125 MHz for ^{13}C spectra), with the deuterium signal of the solvent as the lock and TMS as the internal standard. Chemical shifts (δ) and coupling constants (J) are given in ppm and Hz, respectively. L1, L2, L3, L4, L7 are available in commercial sources. Compound L9[1] and L6[2] has been described previously.

1.1. Synthesis of 3-((1R,4R)-4-(2-(4-(3-cyano-5-fluorophenyl)piperazin-1-yl)ethyl)cyclohexyl)-1,1-dimethylurea (L8)

410 mg (1.1 mmol) 3-(4-(2-((1r,4r)-4-aminocyclohexyl)ethyl)piperazin-1-yl)-5-fluorobenzonitrile[1] was suspended in 50 ml of DCM. 695 µl (5 mmol) of TEA was added to the reaction mixture. Triphosgene (120 mg, 0.40 mmol) was dissolved in 5 ml of DCM and dropped to the previous mixture. The reaction mixture was stirred at room temperature for 1 hour. On the next step dimethylamine hydrochloride (410 mg, 5 mmol) and TEA (695 µl, 5 mmol) were added. The reaction was continued for 20 hours at room temperature. The reaction mixture was filtered and the filtrate was washed with water. The phases were separated and the organic phase was dried over Na_2SO_4. The crude material was purified by flash chromatography, eluting with DCM: MeOH (0-5%). 120 mg (25 %) white solid was obtained. ^1H NMR (500 MHz, CD_3OD) *δ* 7.45 (s, 1H), 7.39 (s, 1H), 7.31 (s, 1H), 5.77 (d, *J*=7.9 Hz, 1H), 3.48 (tdt, *J*=11.6, 7.8, 3.9 Hz, 1H), 3.35–3.31 (m, 4H), 2.86 (s, 6H), 2.65–2.57 (m, 4H), 2.46–2.39 (m, 2H), 1.89 (d, *J*=10.3 Hz, 2H), 1.80 (d, *J*=12.4 Hz, 2H), 1.45 (dd, *J*=15.4, 6.9 Hz, 2H), 1.25 (dd, *J*=24.8, 12.4 Hz, 3H), 1.11–1.01 (m, 2H). ^{13}CNMR (125 MHz, CD_3OD) *δ* 159.08, 151.68, 132.29 (q, J=32.9 Hz), 126.62, 124.45, 122.28, 120.67, 117.62, 117.28 (dd, *J*=8.5, 4.3 Hz), 114.85 (dd, *J*=8.5, 4.3 Hz), 113.79, 56.14, 52.45, 50.10, 49.99, 46.98, 35.34, 35.11, 35.10, 33.26, 33.01, 32.98, 32.04 HRMS (ESI) $(M+H)^+$ calcd for $C_{23}H_{33}N_5OF_3^+$, 452.2637; found 452.2634

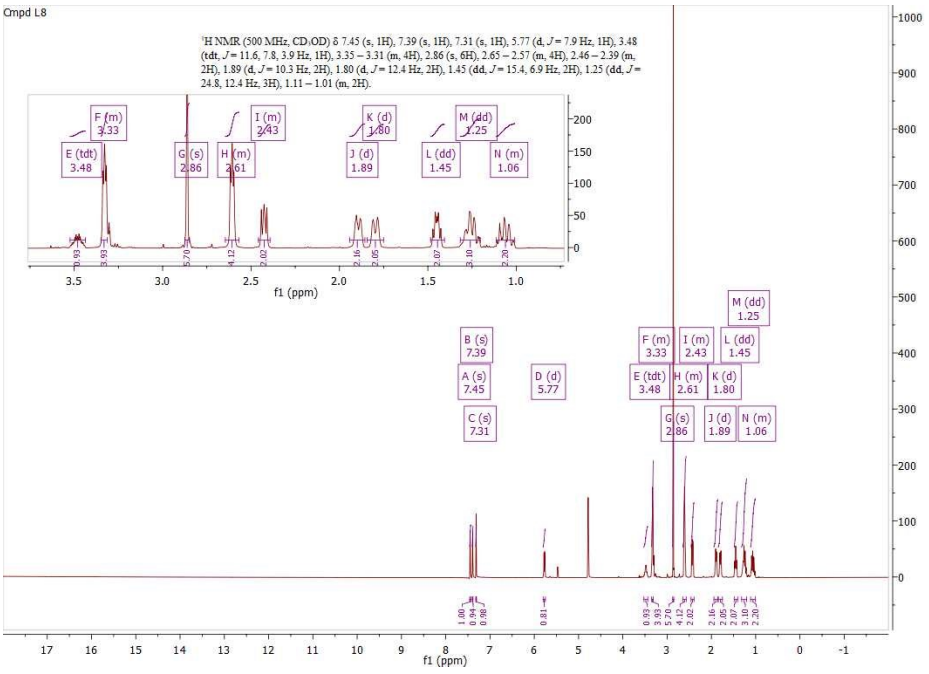

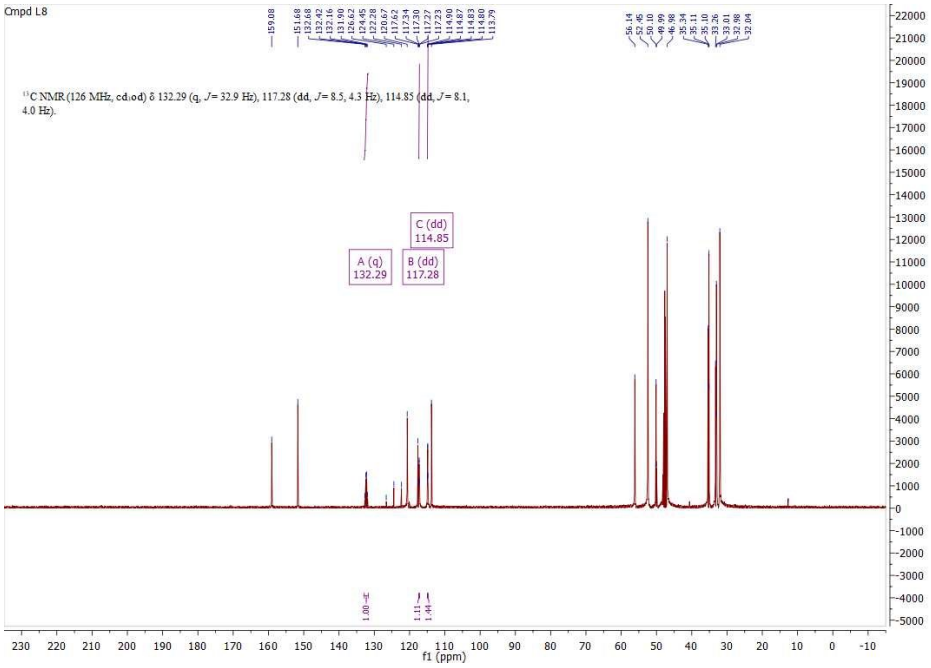

1.2. Synthesis of 3,3-dimethyl-1-[(1R,4R)-4-{2-[4-(2-methoxyphenyl)piperazin-1-yl]ethyl}cyclohexyl]urea (L5)

400 mg (1.26 mmol) (1r,4r)-4-{2-[4-(2-methoxyphenyl)piperazin-1-yl]ethyl}cyclohexan-1-amine[2] was suspended in 50 ml of DCM. 695 µl (5 mmol) of TEA was added to the reaction mixture. Triphosgene (145 mg, 0.48 mmol) was dissolved in 5 ml of DCM and dropped to the previous mixture. The reaction mixture was stirred at room temperature for 1 hour. On the next step dimethylamine hydrochloride (410 mg, 5 mmol) and TEA (695 µl, 5 mmol) were added. The reaction was continued for 20 hours at room temperature. The reaction mixture was filtered and the filtrate was washed with water. The phases were separated and the organic phase was dried over Na_2SO_4. The crude material was purified by flash chromatography, eluting with DCM: MeOH (0-5%). 160 mg (33 %) white solid was obtained. ^{1}H NMR (500 MHz, DMSO-d_6) δ 7.05–6.96 (m, 2H), 6.96–6.87 (m, 2H), 3.79 (s, 3H), 3.53 (dd, *J*=25.7, 12.3 Hz, 4H), 3.36 (tt, *J*=11.5, 3.9 Hz, 1H), 3.24–3.06 (m, 4H), 3.00–2.86 (m, 2H), 2.75 (s, 6H), 1.75 (ddd, *J*=24.4, 13.2, 3.6 Hz, 4H), 1.57 (dt, *J*=11.6, 6.9 Hz, 2H), 1.21 (qd, *J*=12.1, 3.1 Hz, 3H), 1.04–0.91 (m, 2H). ^{13}C NMR (125 MHz, dmso) δ 157.49, 151.80, 139.25, 123.43, 120.77, 118.22, 116.78, 114.46, 111.90, 55.27, 53.84, 51.18, 51.11, 49.13, 46.98, 35.76, 34.38, 32.54, 31.41, 29.99. HRMS (ESI) $(M+H)^+$ calcd for $C_{22}H_{37}N_4O_2^+$, 389.2932; found 389.2939

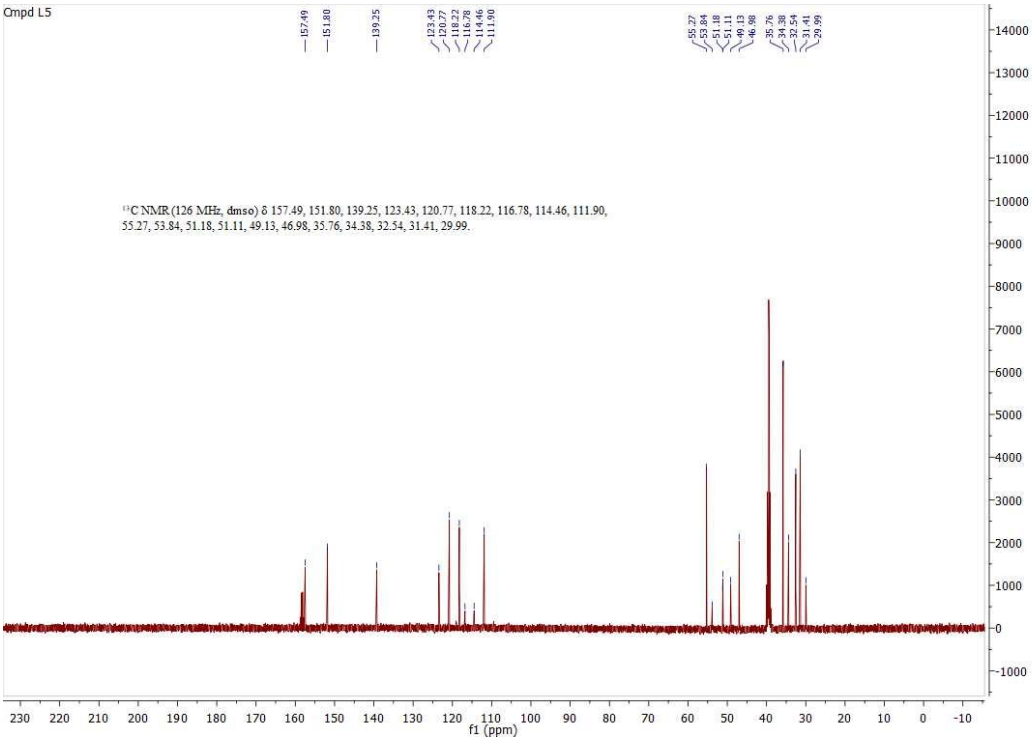

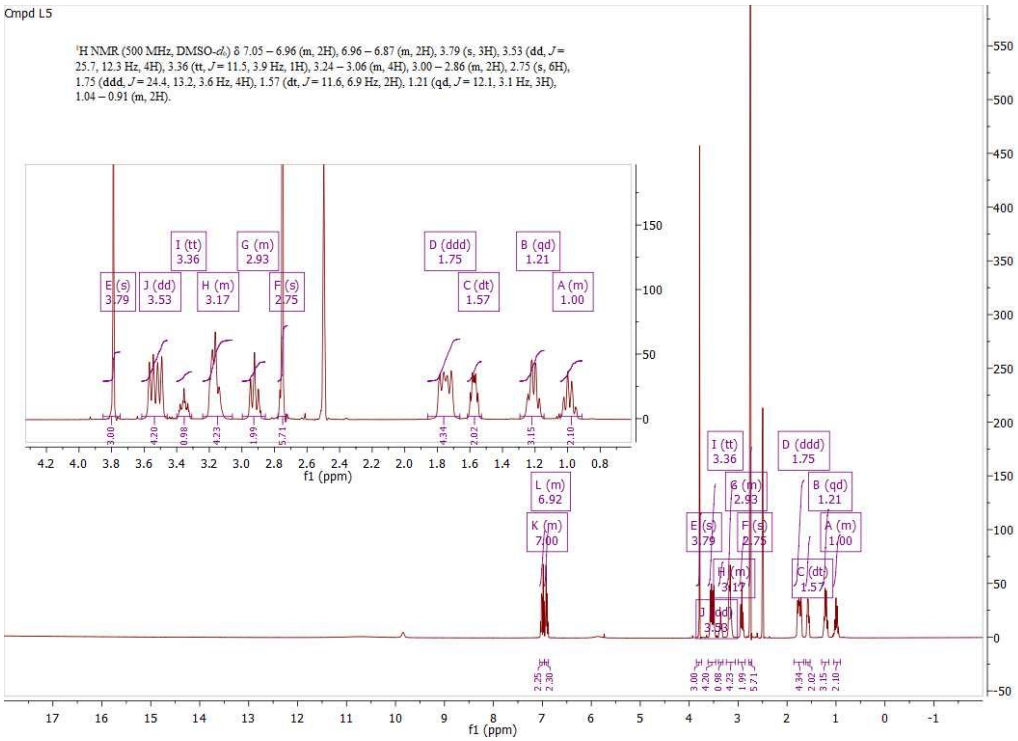

1.3. Materials for in vitro experiments

Tissue culture reagents, if not stated otherwise, were obtained from Life Technologies (now Thermo Fisher Scientific, Waltham, MA USA), while other chemicals were from Sigma-Aldrich (St. Louis, MO, USA) or Merck-Millipore (Darmstadt, Germany). [3H]raclopride was obtained from Perkin Elmer (Waltham, MA, USA).

1.4. Competitive receptor binding on human D2 and D3 receptors

Membrane aliquots of CHO-K1 cells (Eurofins DiscoverX Corporation, USA) expressing human recombinant D2 or D3 receptors were thawed and washed in binding buffer (50 mM Tris-HCl, 5 mM $MgCl_2$, 5 mM KCl, 1 mM $CaCl_2$, 120 mM NaCl, 1 mM EDTA, pH=7.4) and the assay was performed using tritiated raclopride around respective K_d at 25° C. Nonspecific binding was determined in the presence of excess haloperidol. Incubation time was 120 minutes. At the end of incubation, samples were filtered through UniFilter GF/B using a Filtermate Harvester (PerkinElmer) and washed four times with ice cold binding buffer. The plate was dried at 40°C for 60 mins and 40 µl Microscint-20 scintillation cocktail (PerkinElmer, Waltham, MA, USA) was added to each well. Radioactivity was determined in a TopCount NXT scintillation counter (PerkinElmer).

1.5. cAMP measurement

Human D2 receptor expressing cAMP Hunter cell lines (Eurofins DiscoverX Corporation,USA) were expanded from freezer stocks according to standard procedures. Cells were seeded in a total volume of 20 µL into white walled, 384-well microplates and incubated at 37°C for the appropriate time prior to testing. cAMP modulation was determined using the DiscoverX HitHunter cAMP XS+ assay. For agonist determination, cells were incubated with sample in the presence of EC80 forskolin to induce response. Media was aspirated from cells and replaced with 15 µL 2:1 HBSS/10mM Hepes : cAMP XS+ Ab reagent. Intermediate dilution of sample stocks was performed to generate 4X sample in assay buffer containing 4x EC80 forskolin. 4. 5 µL of 4x sample was added to cells and incubated at 37°C or room temperature for 30 or 60 minutes. Final assay vehicle concentration was 1%. For antagonist determination, cells were pre-incubated with sample followed by agonist challenge at the EC80 concentration. Media was aspirated from cells and replaced with 10 µL 1:1 HBSS/Hepes : cAMP XS+ Ab reagent. 5 µL of 4X compound was added to the cells and incubated at 37˚C or room temperature for 30 minutes. 5 µL of 4X EC80 agonist forksolin was added to cells and incubated at 37˚C or room temperature for 30 or 60 minutes.

Flp-in HEK 293 cells (Thermo Fisher Scientific, USA) expressing recombinant human D3 receptor and adenylyl cyclase 5 were suspended in assay buffer and distributed into white, half-well 96-well microplates. In antagonist measurements, cells were preincubated for 15 min with assay buffer (140 mM NaCl, 5 mM KCl, 10 mM HEPES, 2 mM $CaCl_2$, 2 mM $MgCl_2$, 10 mM glucose, 0.1 mM 3-isobutyl-1-methylxanthine and 0.1% bovine serum albumin; pH=7.4) or various concentrations of test compounds. Next, cells were incubated with assay buffer or various concentrations of the test compounds, or in antagonist studies, appr. EC_{80} concentration of dopamine for 20 min. After incubating the cells for 30 min with 2 µM forskolin cell stimulation was stopped by adding detection reagents of HTRF cAMP Dynamic2 kit (Cisbio, Codolet, France). The HTRF signal was quantified with a PHERAstar FS plate reader (BMG Labtech, Ortenberg, Germany) using standard HTRF settings. All incubations were performed at room temperature.

1.6. β-arrestin recruitment assay.

PathHunter (DiscoverX, Fremont, CA, USA) CHO-K1 cells expressing tagged human dopamine D2 and D3 receptors and tagged β-arrestin-2 were seeded into 96-well black-walled clear bottom tissue culture plates in CP2 media (DiscoverX) and incubated overnight in humidified atmosphere with 5% CO_2 at 37°C. Next day test compounds or vehicle diluted in CP2 reagent were added to cells, in antagonist studies followed by an EC_{80} concentration of dopamine after 30 minutes and incubated for 90 min at 37°C. Next, detection solution prepared from PathHunter Detection Kit (DiscoverX) was added to cells followed by incubation in dark for 60 min at room temperature. Luminescence was measured with a PHERAstar FS plate reader.

1.7. Model building

Active state homology models of the hD2 and hD3 receptor coupled with the α subunit of G_o were created following the chimeric homology modelling approach used by GPCRdb.[3] In order to minimize the extent of modelling at the receptor-signalling protein coupling interface, we selected the $5HT_{1B}$ – G_o structure complex (PDB: 6G79)[4] as receptor main template which is coupled with the signalling protein. In both models, the inactive hD2/hD3 loops were swapped in place of the main template loops respectively. MODELLER[5] was used to model residues without coordinates and Schrödinger's Prime[6] was used to remodel regions with steric clashes. The inactive state model was downloaded from GPCRdb (gpcrdb.org/structure). Next, ligands were docked to the models with Glide[7,8] SP protocol applying default settings and minimization took place in Schrödinger's Maestro[9].

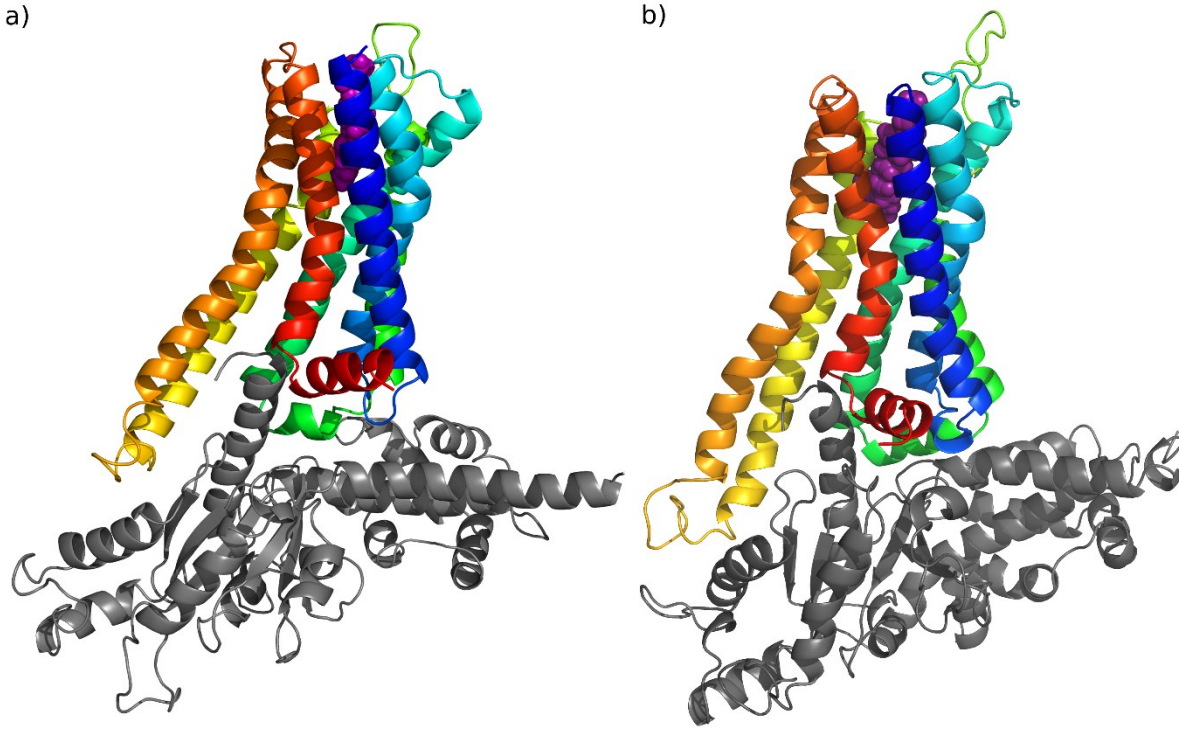

Figure S1: Homology models: a) hD2-G_o b) hD3-G_o models with bound cariprazine. The proteins are represented as cartoons, the receptor is rainbow coloured and the transducers are grey. The bound ligands are shown as purple spheres.

1.8. Molecular dynamics simulations

All partial or full agonists were modelled in the transducer bound models, while the antagonist was modelled in the inactive hD2 (PDB ID: 6CM4[10]), the inactive hD3 X-Ray structure (PDB ID: 3PBL[11]) and also in the activated structure models, however without the coupled transducer. The complexes were neutralized and solvated in pre-equilibrated POPC lipid bilayer with TIP3P waters and the NaCl concentration was adjusted to 0.15 M. The transducer bound systems contain approximately 120000-150000, while the other models approximately 65000 atoms. All atoms were explicitly modelled with OPLS3[12] force field parameters during the molecular dynamics simulations. Schrödinger's protocol for membrane proteins was followed during the equilibration containing 3 NVT and 4 NPT steps; the temperature is increased from 10 K to 310 K and all restraints are lifted for the final steps. The input files for the equilibration were generated with the relax_membrane.py script available in the Schrödinger Suite. Semi-isotropic NPT ensemble was applied for the 500 ns production runs with a 13.5 Å short-range electrostatic cutoff distance and 2 fs time steps with the RESPA integrater using Desmond.[13] The temperature was controlled with the Nose-Hoover chain method with 1 ps relaxation time, while the pressure was stabilized at 1.01325 bar with the Martyna-Tobias-Klein barostat with 2 ps relaxation time. The simulations were run in parallel at 310K for 500 ns.

1.9. Analysis of trajectories

The analysis was carried out with the analyze_simulation.py and analyze_trajectories.py scripts provided by Schrödinger for every tenth frame of the last 400 ns of the simulations and the results were averaged for the parallel runs.
For the protein-ligand interaction analysis we measured the direct and water mediated hydrogen bonds, hydrophobic interactions including aromatic interactions and ionic interactions excluding the hydrogen bonds. The latter one was not dominant in any case as we observed strong hydrogen bonds between the positively charged centre of the ligand and the conserved aspartate residue; therefore, we consider this interaction as a hydrogen bond formation. Interactions which were displayed at least 20% of the frames in average for at least one ligand were included in Fig1 and Fig2. Due to clarity, on the figures we summed up the direct and water mediated hydrogen bonds for the residues. Interactions with halogens are not accounted for in the default protein-ligand interaction analysis, therefore we assess potential interaction with the halogens by measuring the halogen-heavy atom distance (O, N) and apply a 4.0 Å cut-off.
Complete linkage hierarchical clustering was carried out with the MDtraj python package applying a 0.15 nm RMSD cut-off for the OBP atoms.

2. Results and Discussion

2.1. Binding data

Table S1. Binding affinities (with s.d. values) measured for the hD2 and hD3 receptors.

	SBP	Compound code	pK_i hD2	pK_i hD3	Selectivity
	-	1	6.80 (0.01)	7.07 (0.02)	1.86
OBP1	SBP1	2	8.70 (0.11)	9.50 (0.34)	6.31
	SBP2	3	8.00 (0.13)	8.63 (0.29)	4.27
	-	4	6.19 (0.05)	5.88 (0.08)	0.49
OBP2	SBP1	5	8.09 (0.10)	8.79 (0.13)	1.28
	SBP2	6	8.67 (0.10)	8.20 (0.18)	1.32
	-	7	6.42 (0.01)	6.67 (0.09)	1.78
OBP3	SBP1	8	7.92 (0.01)	9.01 (0.09)	12.30
	SBP2	9	7.46 (0.01)	8.42 (0.07)	9.12

2.2. Correlation between binding and functional data

The correlation between binding (Table S1) and functional data measured in both G-protein (Table 1) and β-arrestin (Table 2) modalities were analyzed for compounds **1**-**9** on both hD2 and hD3 receptors. In general, efficacy data measured on both receptors in both modalities followed similar trends as receptor affinities. In the case of the hD2 receptor, the correlation coefficient (r) between the binding affinity and efficacy was 0.74 and 0.85 for the G-protein and β-arrestin data, respectively. In the case of the hD3 receptor, the correlation coefficient (r) between the binding affinity and efficacy was 0.79 and 0.90 for the G-protein and β-arrestin data, respectively. Interestingly, we found that slope values were higher for the hD2 than that of the hD3 receptors indicating that coupling might be different even for related GPCRs.

2.3. RMSD and RMSF values calculated from the MD simulations

Table S2. Average ligand and protein backbone RMSD and RMSF values calculated from the parallel MD simulations. Coding refers to the compound number and parallel run as follows: L2-1 means first parallel run of compound (ligand) 2.

	Protein backbone RMSD / Å		Protein backbone RMSF / Å		Ligand RMSD / Å	
Ligand code	hD2	hD3	hD2	hD3	hD2	hD3
L2-1	2.6	2.6	1.7	1.6	1.5	3.1
L2-2	3.8	2.4	2.0	1.5	2.3	2.7
L3-1	2.8	3.2	1.9	1.9	2.2	2.4
L3-2	2.9	2.6	1.8	1.6	1.5	1.3
L5-1	2.6	2.8	1.9	1.7	2.3	2.1
L5-2	2.8	2.9	2.0	1.7	2.0	1.4
L6-1	2.8	3.0	1.9	1.7	2.4	1.7
L6-2	3.3	2.8	2.3	1.7	2.1	2.0
L8-1	2.3	1.4	1.3	1.0	1.0	1.0
L8-2	1.7	2.0	1.1	1.2	1.6	1.8
L9-1	2.4	2.9	1.9	1.8	1.7	1.6
L9-2	3.7	2.7	2.0	1.7	2.7	1.3

2.4. Interaction patterns

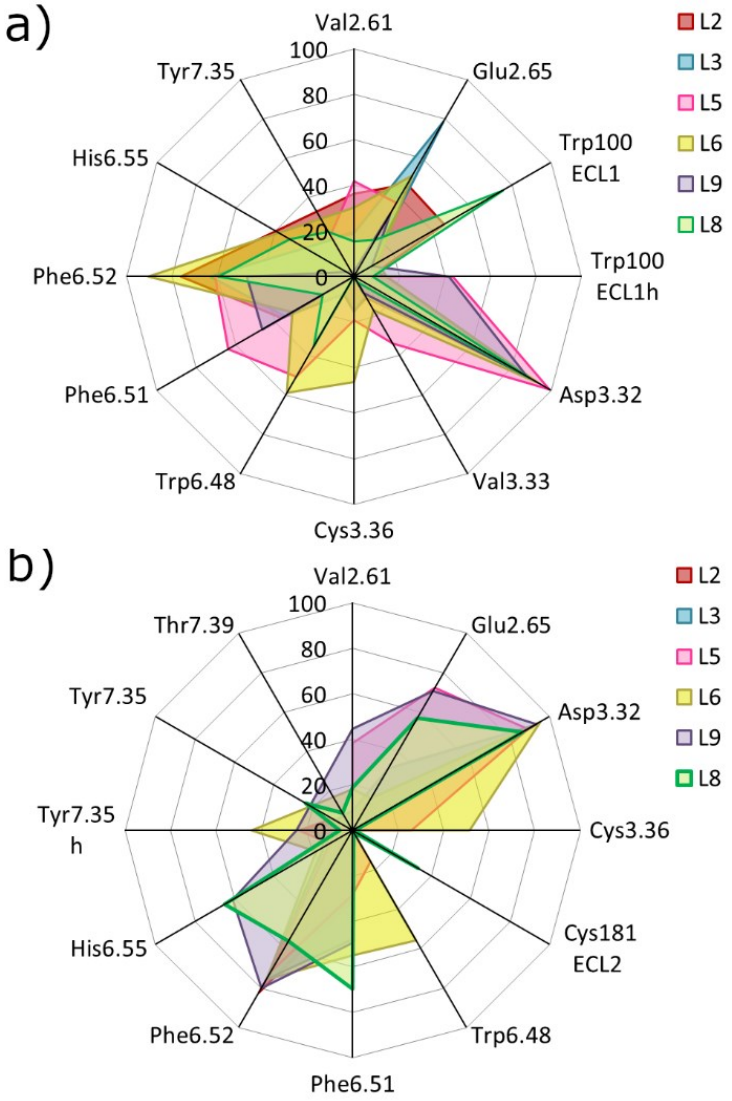

Figure S2: Most abundant interactions calculated from the parallel MD simulations for the (a) hD2 and (b) hD3 receptors. Numbering refers to the main article, L2 indicates simulation with ligand 2. The analysis considered H-bonds, salt bridges, hydrophobic interactions (including aromatic interactions), however it did not account for halogen bonds. If a residue forms both hydrophobic interactions and hydrogen bonds, the former one is indicated by h after the residue name. For the potential halogen bond interaction with Ser5.42 see **Figure S4**.
Available mutational data for key residues (Asp114$^{3.32}$Ala, Phe389$^{6.51}$Ala, Phe390$^{6.52}$Ala, Glu95$^{2.65}$Ala) for different ligands like dopamine, risperidone, MLS1547, SB269652 support that these interactions are essential for binding and functional activity.[10,14–16] Likewise, mutation of Trp100^{ECL1}Ala increases the association and dissociation of antagonist ligand risperidone.[17]

2.5. hD2 haloperidol, risperidone and bromocriptine structure overlay

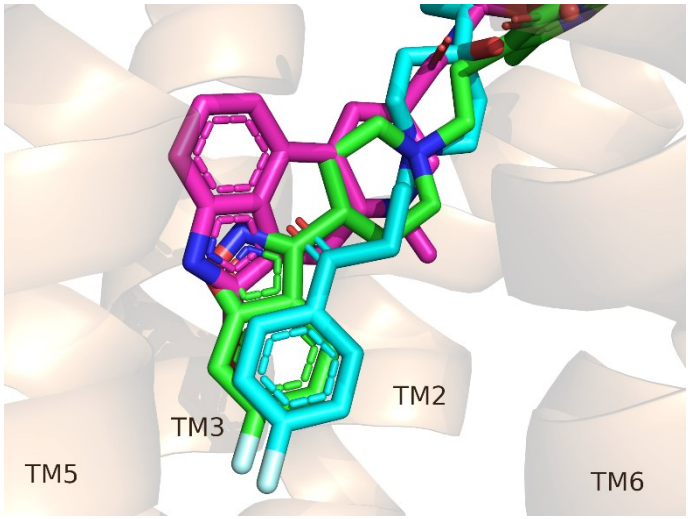

Figure S3: The aligned risperidone[10] (green, antagonist), haloperidol[18] (cyan, antagonist) and bromocriptine[19] (magenta, agonist) structures. The antagonists extend to a deeper subpocket of the receptor compared to the agonist and the plane of their rings in the OBP rotates with app. 35° compared to bromocriptine.

2.6. Distance from Ser$^{5.42}$

The distance between the oxygen of Ser$^{5.42}$ and the halogen atoms of the agonists were followed during the dynamics. The frequency of potential interactions defined as a distance smaller than 4 Å are shown on FigureS2.

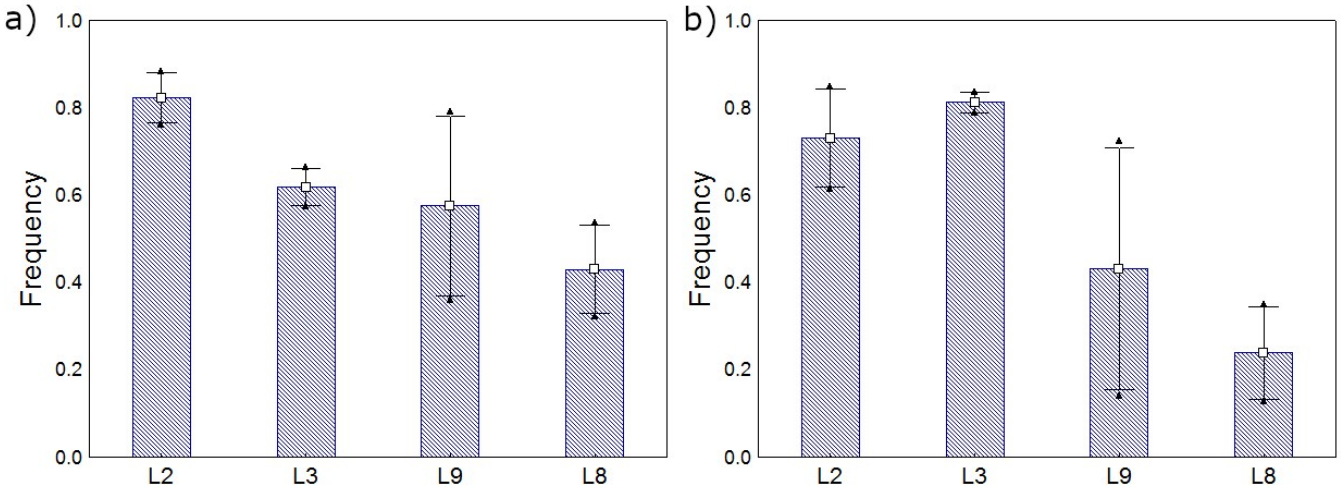

Figure S4: Frequency of potential interaction between Ser$^{5.42}$ and the agonists' halogen atoms for the (a) hD2 and (b) hD3 receptor. L9 is a very weak partial agonist in both the hD2 and hD3 receptor that might contribute to the observed high standard deviation between the parallel runs.

The data suggests that the antagonist L8 tilts away from TM5 more often compared to the agonists (L2, L3, L9), although this phenomenon is more pronounced for hD3. We have to note here that the deviation is high especially for L9, therefore the difference between L9 and L8 is not significant. The smaller gap between L9 and L8 in the hD2 receptor and the high deviation in both receptors might be contributed to the very weak partial agonist nature of L9 observed in our experiments. In line with these findings we would like to draw attention to a potential halogen bond for these ligands, however we do not believe that solely this potential interaction drives the functional behaviour.

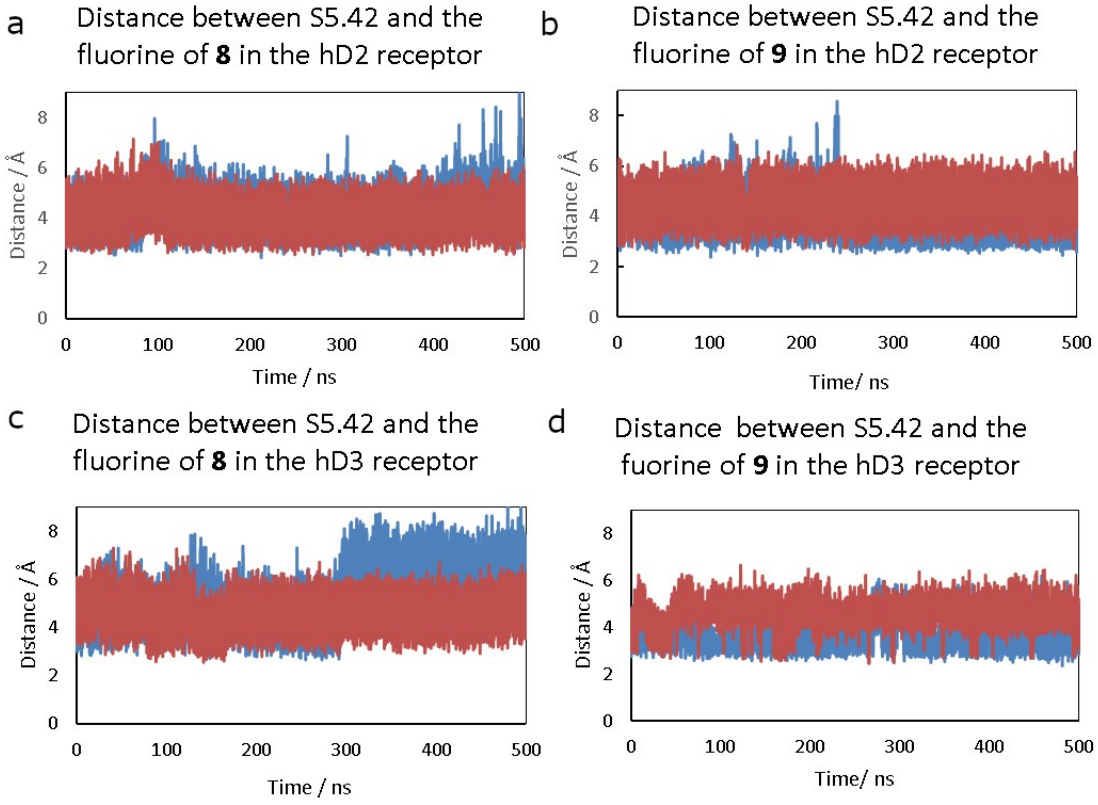

Figure S5: Distance between Ser5.42 and the fluorine of compound **8** (a,c) and compound **9** (b,d) in the hD2 and hD3 receptor respectively.

The time dependence also reveals that the distance fluctuates for both ligands and in only one case did we observe a major change compared to the original position (for compound **8** in hD3). This suggests that both ligands fluctuate between conformations closer and farther to Ser5.42 during the simulations. However, we believe this behaviour is in line with the experimental results, as compound **9** is a very weak partial agonist, therefore even slight preference of one OBP conformation over the other might be a key. However, we do not believe that this specific interaction drives completely the functional behaviour, it is just rather an indication of the different behaviour observed in our MDs.

2.7. Binding mode of compound 7, 8 and 9

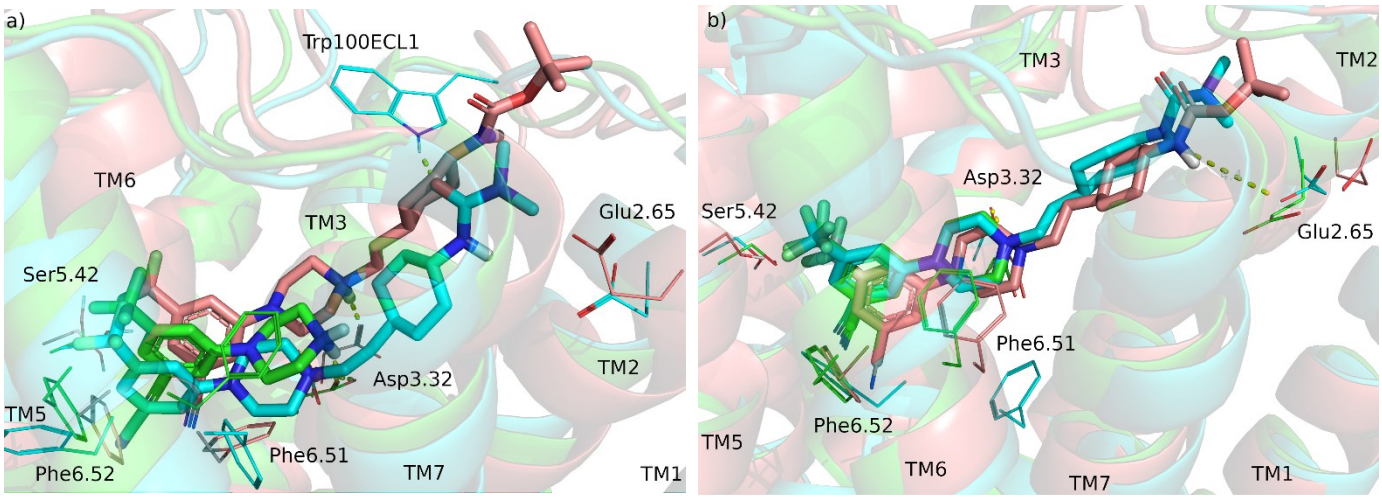

Figure S6: The binding mode of 7 (green) from docking and 8(cyan) and 9(light pink) from the MD simulation in the hD2 (a) and hD3 (b) receptor. Line representation highlights some major interacting residues.

The antagonist OBP binder **7** binding mode is close (hD2) or completely overlaps (hD3) with the SBP containing antagonist **8** likely in connection with their similar functional behaviour.

2.8. OBP repositioning in the 5-HT_{2B} structure

Aligning the X-Ray structure of LSD[20] and ergotamine[21] in the 5-HT2B receptor reveal that the orthosteric binding motif is positioned differently in the orthosteric site likely in connection with their different functional profile.

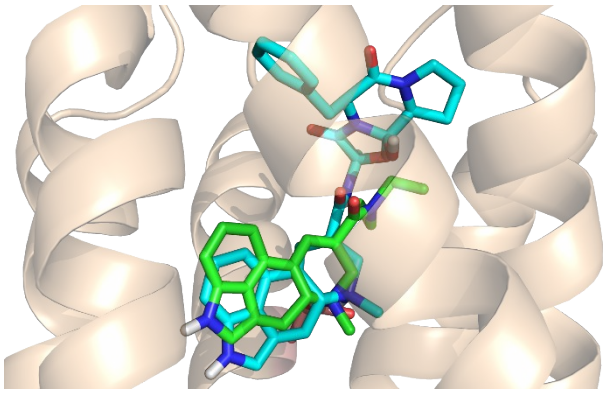

Figure S7: The aligned LSD[20] and ergotamine[21] 5-HT_{2B} X-Ray structure

3. References

1 É. Ágai-Csongor, G. Domány, K. Nógrádi, J. Galambos, I. Vágó, G. M. Keserű, I. Greiner, I. Laszlovszky, A. Gere, É. Schmidt, B. Kiss, M. Vastag, K. Tihanyi, K. Sághy, J. Laszy, I. Gyertyán, M. Zájer-Balázs, L. Gémesi, M. Kapás and Z. Szombathelyi, *Bioorg. Med. Chem. Lett.*, 2012, **22**, 3437–3440.

2 J. Shonberg, C. Draper-Joyce, S. N. Mistry, A. Christopoulos, P. J. Scammells, J. R. Lane and B. Capuano, *J. Med. Chem.*, 2015, **58**, 5287–5307.

3 G. Pándy-Szekeres, C. Munk, T. M. Tsonkov, S. Mordalski, K. Harpsøe, A. S. Hauser, A. J. Bojarski and D. E. Gloriam, *Nucleic Acids Res.*, 2018, **46**, D440–D446.

4 J. García-Nafría, R. Nehmé, P. C. Edwards and C. G. Tate, *Nature*, 2018, **558**, 620–623.

5 A. Šali and T. L. Blundell, *J. Mol. Biol.*, 1993, **234**, 779–815.

6 M. P. Jacobson, D. L. Pincus, C. S. Rapp, T. J. F. Day, B. Honig, D. E. Shaw and R. A. Friesner, *Proteins Struct. Funct. Bioinforma.*, 2004, **55**, 351–367.

7 R. A. Friesner, J. L. Banks, R. B. Murphy, T. A. Halgren, J. J. Klicic, D. T. Mainz, M. P. Repasky, E. H. Knoll, M. Shelley, J. K. Perry, D. E. Shaw, Perry, Francis and P. S. Shenkin, *J. Med. Chem.*, 2004, **47**, 1739–1749.

8 Schrödinger Release 2017-4: Glide, Schrödinger, LLC, New York, NY, 2017

9 Schrödinger Release 2017-4: Maestro, Schrödinger, LLC, New York, NY, 2017

10 S. Wang, T. Che, A. Levit, B. K. Shoichet, D. Wacker and B. L. Roth, *Nature*, 2018, **555**, 269–273.

11 E. Y. T. Chien, W. Liu, Q. Zhao, V. Katritch, G. W. Han, M. A. Hanson, L. Shi, A. H. Newman, J. A. Javitch, V. Cherezov and R. C. Stevens, *Science*, 2010, **330**, 1091–5.

12 E. Harder, W. Damm, J. Maple, C. Wu, M. Reboul, J. Y. Xiang, L. Wang, D. Lupyan, M. K. Dahlgren, J. L. Knight, J. W. Kaus, D. S. Cerutti, G. Krilov, W. L. Jorgensen, R. Abel and R. A. Friesner, *J. Chem. Theory Comput.*, 2016, **12**, 281–296.

13 Schrödinger Release 2017-4: Desmond Molecular Dynamics System, D. E. Shaw Research, New York, NY, 2017. Maestro-Desmond Interoperability Tools, Schrödinger, New York, NY, 2017

14 W. Cho, L. P. Taylor, A. Mansour and H. Akil, *J. Neurochem.*, 1995, **65**, 2105–2115.

15 N. Tschammer, M. Dörfler, H. Hübner and P. Gmeiner, *ACS Chem. Neurosci.*, 2010, **1**, 25–35.

16 J. R. Lane, P. Donthamsetti, J. Shonberg, C. J. Draper-Joyce, S. Dentry, M. Michino, L. Shi, L. López, P. J. Scammells, B. Capuano, P. M. Sexton, J. A. Javitch and A. Christopoulos, *Nat. Chem. Biol.*, 2014, **10**, 745–752.

17 J. R. Lane, A. M. Abramyan, P. Adhikari, A. C. Keen, K. H. Lee, J. Sanchez, R. K. Verma, H. D. Lim, H. Yano, J. A. Javitch and L. Shi, *Elife*, 2020, **9**, e52189.

18 L. Fan, L. Tan, Z. Chen, J. Qi, F. Nie, Z. Luo, J. Cheng and S. Wang, *Nat. Commun.*, 2020, **11**, 1–11.

19 J. Yin, K. Y. M. Chen, M. J. Clark, M. Hijazi, P. Kumari, X. chen Bai, R. K. Sunahara, P. Barth and D. M. Rosenbaum, *Nature*, 2020, **584**, 125.

20 D. Wacker, S. Wang, J. D. McCorvy, R. M. Betz, A. J. Venkatakrishnan, A. Levit, K. Lansu, Z. L. Schools, T. Che, D. E. Nichols, B. K. Shoichet, R. O. Dror and B. L. Roth, *Cell*, 2017, **168**, 377-389.e12.

21 D. Wacker, C. Wang, V. Katritch, G. W. Han, X.-P. Huang, E. Vardy, J. D. McCorvy, Y. Jiang, M. Chu, F. Y. Siu, W. Liu, H. E. Xu, V. Cherezov, B. L. Roth and R. C. Stevens, *Science*, 2013, **340**, 615–9.